Image Analysis for Electron Microscopy of Muscle Fibres

C.H. Yoon, P.J. Bones and R.P. Millane
Department of Electrical and Computer Engineering
University of Canterbury
Private Bag 4800, Christchurch, New Zealand
rick@canterbury.ac.nz

Abstract

An automated image analysis system for determination of myosin filament orientations in electron micrographs of muscle cross-sections is described. Analysis of the distribution of the orientations is important in studies of muscle structure, particularly for interpretation of x-ray diffraction data. Filament positions are determined by filtering with a point spread function that incorporates the local symmetry in an image. Filament orientations are determined by correlation with a template that incorporates the salient filament characteristics and the orientations classified using a Gaussian mixture model. Application to micrographs and comparison with manual classification of orientations shows that the system is effective.

1. Introduction

Vertebrate muscle fibers contain the contractile proteins myosin and actin which are organised into long thin strands known as myofibrils. The myofibrils exhibit a striated pattern and the repeating unit is known as the sarcomere, which is the basic contractile unit of muscle [1]. The structure of this complex system is studied by both electron microscopy and x-ray diffraction. Myosin filaments pack in a semiregular lattice and can be imaged directly by electron microscopy of thin transverse sections (about 50nm thick) through the so-called bare region on each side of the M-band. In this region, myosin filaments are roughly triangular in shape and devoid of actin filaments and other molecular components so that such micrographs are ideal for image analysis. Luther and Squire [2] determined, by visual analysis of micrographs, that in many muscles, such as those from frogs, the myosin filaments adopt one of two different orientations that are distributed in a semi-systematic manner. Using these results, they described some general characteristics of the distribution of orientations which were confirmed by a more quantitative analysis by Millane and Goyal [3]. The myosin filament disorder has implications for the contractile mechanism of the muscle, and a good statistical model of the disorder is needed for rigorous interpretation of x-ray diffraction data from muscle fibres. The micrographs are quite noisy, and manual analysis is slow, tedious, difficult and prone to error, and the accuracy of the results is difficult to assess quantitatively. However, to obtain a good statistical picture of the disorder, it is necessary to analyse a number of micrographs both within and between species. We have therefore developed a method for automated analysis of these kinds of micrographs to allow rapid and quantitative determination of the filament orientations.

Location of the myosin filaments is described in Section 2. In Section 3, determination of the filament orientations is described, and in Section 4 classification of the orientations is described. Results of application of this system to two micrographs are presented in Section 5. Concluding remarks are made in Section 6.

2. Location of filaments

An example micrograph is shown in Fig. 1. It is a thin transverse section through a frog sartorius muscle fibre containing the myosin filaments (the dark regions that can be seen to lie on an approximately triangular lattice). The images used here have pixel values from 0 (black) to 255 (white). There are large variations between images due to many factors such as specimen type, sample preparation, etc. The first step in the analysis is to locate all the myosin filaments inside a myofibril (the ordered region surrounded by an amorphous boundary that can be seen in Fig. 1).

We have previously described an algorithm that uses greyscale morphology to determine the filament locations [4, 5]. This algorithm uses h-dome extraction [6] to locate local maxima in the image. However the result is sensitive to the threshold value h, and the lattice symmetry is used to determine the optimum threshold value. Even with the optimum threshold, the noisy nature of the images means

Proceedings of the Digital Imaging Computing: Techniques and Applications (DICTA 2005)
0-7695-2467-2/05 $20.00 © 2005 **IEEE**

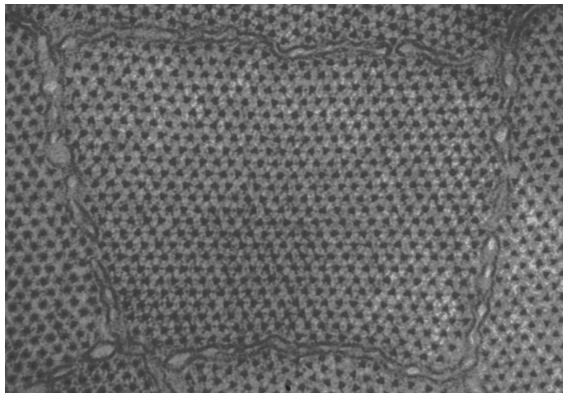

Figure 1: Electron micrograph of a slice of frog sartorius muscle.

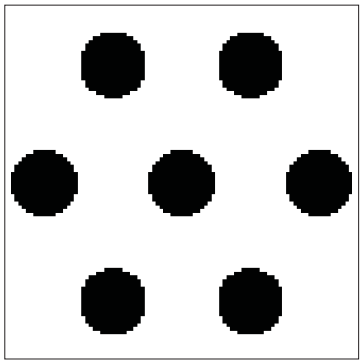

Figure 2: The filter point spread function used to determine the filament positions.

that erroneous maxima are also identified, and these are removed by further iterative morphological processing that also uses the lattice symmetry. The morphological algorithm is quite successful [4, 5], but is quite complex and does not use the lattice symmetry in the most efficient manner.

We have now developed a simpler approach that uses linear filtering with a point spread function (psf) that incorporates the filament size and lattice regularity at the outset. Inspection of Fig. 1 shows that the lattice on which the filaments lie is not regular over large distances but is reasonably regular on a local scale. The variation in the lattice over the entire image is larger but is still rather small. The idea is to use this local symmetry to generate a psf that can be used to filter the whole micrograph image. Formation of the psf is as follows: The user defines the approximate coordinates of the centre of a filament and its six nearest neighbour filaments on the micrograph image. These centre coordinates do not need to be particularly accurate. The twelve nearest neighbour spacings between the filaments are calculated and averaged. The orientations between the twelve nearest neighbour vectors are calculated and averaged modulo 60°. The average spacing and orientation is used to define a psf consisting of seven disks arranged in a hexagon as shown in Fig. 2. The diameter of the disks is set equal to half the average spacing (this is a common feature throughout different muscle micrographs). This then defines the psf for a given image.

The psf is convolved with the image (implemented by multiplying the DFTs of the image and the psf and calculating the inverse DFT), producing a filtered image with distinct intensity peaks at the filament positions and a considerably reduced noise level compared to the original image. The advantage of this approach over the morphological approach is that the constraints of local maxima and local hexagonal symmetry are incorporated into a single step. The result is that a cleaner estimate of the peaks corresponding to the filaments is obtained much more easily. The regional maxima of the filtered image are determined as the connected regions (based on 8-neighbourhoods) of pixels with the same value, whose external boundary pixels all have smaller values. The centroids of the regional maxima structures are the estimates of the filament positions.

It is worth pointing out that, at first sight, these images, such as that shown in Fig. 1, have the appearance of a texture and might be susceptible to analyses such as texture segmentation [7]. However, while the region of a whole myofibril resembles a texture, a delineation of the myosin filaments does not correspond to segmentation of different textures.

3. Determination of filament orientations

Having determined the approximate locations of most of the filaments as described in the previous section, the next step is to estimate the orientation of each filament. The approach used is template matching, which is a common technique for locating parameterised features in images [8]. Inspection of many filaments in micrographs shows that they generally have an approximate equilateral triangular shape. A template is first constructed as a triangle of specified size (edge length). For pixels on the edge of the triangle, the pixel value is set to the fraction of the pixel within the triangle. The basic idea is to correlate the template at different orientations with the image of a filament and take the orientation of the template that gives the maximum correlation as the estimate of the orientation of the filament. Experimentation with the approach showed that better discrimination in the estimated orientations is obtained by modifying the template as follows. Since the filaments in the micrographs do not have sharp edges, a better template is obtained by blur-

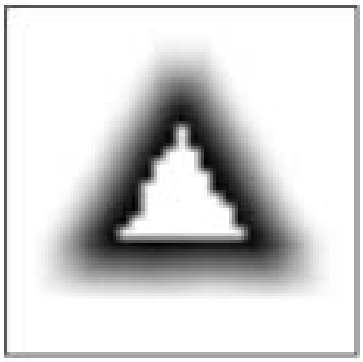

Figure 3: Template used to determine the filament orientations.

ring the triangular template with a square of 5×5 pixels. In addition, a triangular region in the centre of the template is set to zero such that the inside border of the template has a single line of pixels of the maximum value of the template. This appears to help because some filaments have holes in the centre and because the central region of the mask tends to swamp the correlation. A template is illustrated in Fig. 3.

The best discrimination is obtained if the template size and position accurately correspond to the size and position of the filament in the image. Since the filament positions and sizes are known only approximately, a four-dimensional search is conducted over a range of positions (x and y), sizes (represented by the template edge length s) and orientations θ of the template. The range of orientations used is $\{0, \triangle\theta, 2\triangle\theta, ..., 120^\circ - \triangle\theta\}$ where $\triangle\theta = 4^\circ$. The range of template edge lengths used is $d_{min} < s < d_{max}$, where the values of d_{min} and d_{max} depend on the raster spacing, but are easily determined for a particular image. The range of positions used also depends on the specific case and an interval of 0.5 pixels is used.

The correlation coefficient is calculated as

$$r(\Delta x, \Delta y, s, \theta) = \frac{1}{n-1} \sum_{i=1}^{n} \left[\frac{t(\Delta x, \Delta y, s, \theta, i) - \mu_t}{\sigma_t} \cdot \frac{f(i) - \mu_f}{\sigma_f} \right] \quad (1)$$

where t and f respectively stands for template and filament image, Δx and Δy are the template shifts (relative to the filament marker), μ and σ are the mean and standard deviation respectively, and the sum is over the n pixels i that overlap in the template and the filament image. The estimate of the filament orientation is then taken as the value of θ that maximises $r(\Delta x, \Delta y, s, \theta)$ over $\Delta x, \Delta y, s$ and θ. Filaments that are less triangular in shape give less reliable orientations and lower correlation coefficients. Filaments with correlation coefficients less than a chosen threshold value are marked as having an unknown orientation. A good threshold value varies between images although a value of 0.75 was found to be suitable in many cases. In addition to the minimum correlation coefficient, the ratio of the maximum to the minimum correlation coefficient over all orientations (at the values of $\Delta x, \Delta y$ and s that maximise r) is also recorded as a measure of the reliability of the orientation estimate.

4. Classification of orientations

As described in the introduction, the myosin filaments in many muscles adopt one of two opposite orientations, and it is the spatial distribution of the two orientations in which we are interested. The difference in orientation, determined as described in the previous section, for oppositely oriented filaments is approximately 60°. As a result of imperfections in the muscle and errors in determining the orientations, the measured orientations do not belong to two groups that are exactly 60° apart. In practice there is a distribution of orientations that tend to fall into two populations. The objective is to classify each filament orientation as belonging to one of two populations which we refer to as *up* and *down*. The underlying distribution of orientations is modelled as a Gaussian mixture consisting of two normal distributions. Since the orientations exist on the finite interval $(0, 120^\circ)$, the normal distributions are wrapped on this interval and denoted by $f(\mu, \sigma, \theta)$ where μ and σ are the mean and standard deviation of the original normal distribution. The model distribution of filaments orientations $f_{model}(\theta)$ is given by

$$f_{model}(\theta) = p_{up} f(\mu_{up}, \sigma_{up}, \theta) + (1 - p_{up}) f(\mu_{down}, \sigma_{down}, \theta), \quad (2)$$

where p_{up} is the fraction of filaments classified as up. The parameters $\mu_{up}, \mu_{down}, \sigma_{up}, \sigma_{down}$, and p_{up} are determined by fitting $f_{model}(\theta_i)$ to the histogram of estimated filament orientations $h(\theta_i)$ over the whole image by minimising the sum of squared errors. Note that for estimated orientations that give a good classification we expect that $\triangle\mu = |\mu_{up} - \mu_{down}| \approx 60^\circ, \sigma_{up} \ll 60^\circ, \sigma_{down} \ll 60^\circ$ and $p_{up} \approx 0.5$. The values of the parameters $\triangle\mu, \mu_{up}, \mu_{down}$ and p_{up} can therefore be used to measure the degree to which the data are consistent with two populations of orientations of this kind. Each orientation interval θ_i is assigned to either population depending on the relative dominance of the densities at that interval, i.e.

$$\theta_i \in \begin{cases} \pi_{up} & \text{if } p_{up} f(\mu_{up}, \sigma_{up}, \theta_i) \geq p_{down} f(\mu_{down}, \sigma_{down}, \theta_i) \\ \pi_{down} & \text{otherwise} \end{cases} \quad (3)$$

where π_{up} and π_{down} represent the up and down classifications, respectively, which minimises the expected number of misclassifications.

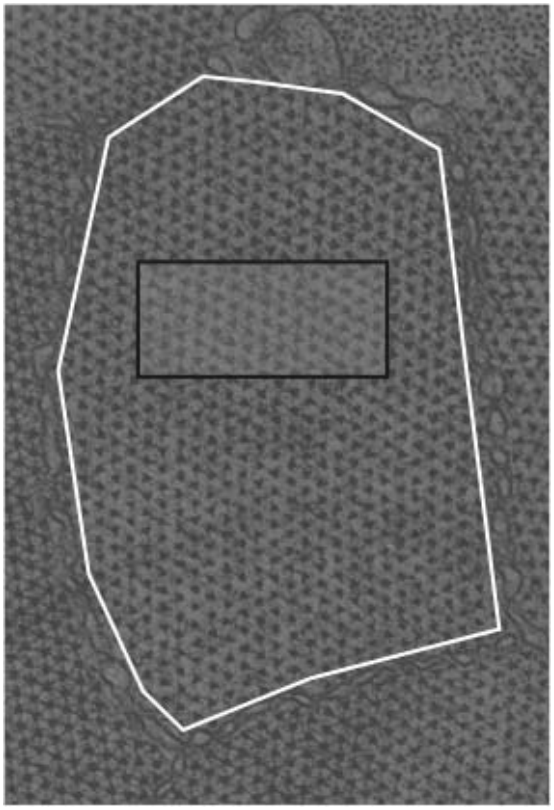

Figure 4: Electron micrograph of frog sartorius muscle. The white border denotes the region of one myofibril which was analysed. The black border denotes the subimage shown in Figs. 6 and 8.

5. Results

The algorithms described above were implemented in Matlab and run on 2.8GHz PC. Examples of the application of the automated image analysis system to micrograph of two different species, frog and turtle are presented in this section. The automatically determined orientations were compared with manually determined orientations. For the manual analysis, a program was used which allows the user to visually fit an equilateral triangle with adjustable position, angle and size to each filament. The manually determined orientations are used to classify the orientations as for the automated method as described above. Orientations that cannot be reliably estimated manually are marked as unknown and are not used in the classification.

Part of a micrograph of a cross-section of frog sartorius muscle [2] is shown in Fig. 4 and the region of one myofibril (inside the white border), which contains 750 filaments, was analysed. The location algorithm described in Section 2 was run. The algorithm took less than one minute to run and located all 750 filaments. A subimage (corresponding to the region outlined in black in Fig. 4) is shown in Fig. 5, together with the region used to define the psf, the psf, the filtered image and the final filament positions.

The filament orientations were determined automatically as described in Section 3. The average time per filament was 0.2s and the orientation analysis for the whole image took two minutes. The orientation distribution is shown in Fig. 6 and two populations are clearly evident. The mean correlation coefficient obtained for all filaments was 0.80. Using a correlation threshold of 0.75, 699 of the orientations (93%) were above the threshold. The manual analysis found only 580 (77%) reliable orientations. Orientations with a correlation coefficient below the threshold or which could not be determined manually are labelled "bad" and are not included in the analysis. Fitting the mixture model gave $\triangle\mu = 62°$, $\sigma_{up} = 11°$, $\sigma_{down} = 9°$ and $\rho_{up} = 0.50$, indicating that the data are consistent with two populations of filament orientations. The mixture model is shown in Fig. 6. Classification of the orientations was performed as described in Section 4 and took 2 seconds for the whole image. The orientations and their classification are illustrated in Fig. 7.

The filament orientations were determined manually and classified automatically as described above. A comparison of the results of the manual and automatic classifications are shown in Table 1. As seen in the table, the automatically determined orientations are consistent overall with the manual determinations. Of the 699 automatically determined orientations, 554 (80%) agree with the manually determined orientations, only 4 ($< 1\%$) have the opposite orientation, and the remaining 141 (20%) could not be determined manually. As expected, there is more variety in the identification of bad filaments. This appears to be a good result overall for the automatic classification, remembering that the manual classification is not a "gold standard," and in fact the automatic method is probably more accurate than the manual method.

The second example is a micrograph of a cross-section of turtle muscle containing 150 filaments shown in Fig. 8. The myosin filaments in this image are not clear and hence manual analysis is difficult. The results of the filament location on a subimage are shown in Fig. 9. 149 out of the 150 filaments were located and the locations in the subimage are shown in Fig. 9c.

The filament orientations were determined automatically giving a mean correlation coefficient of 0.75. Using a corre-

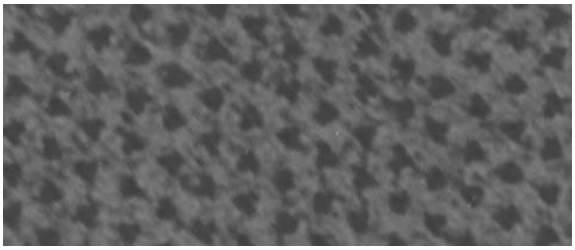

(a)

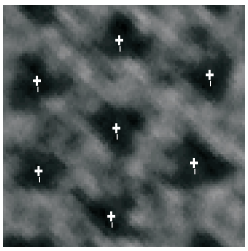

(b)

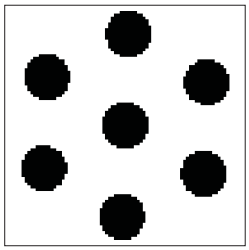

(c)

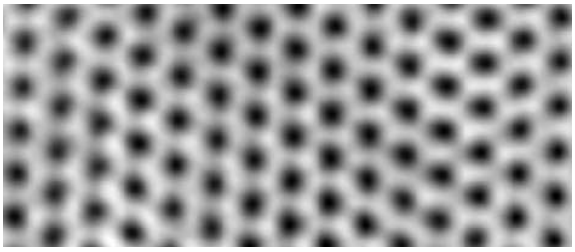

(d)

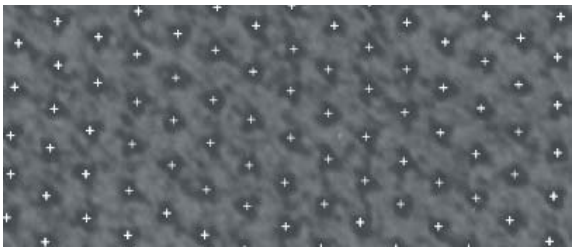

(e)

Figure 5: (a) Original subimage, (b) user input, (c) psf, (d) filtered subimage and (e) determined filament posit- ions.

lation threshold of 0.65, 133 of the orientations (89%) were above the threshold. Fitting the mixed Gaussian model gave $\triangle\mu = 61°$, $\sigma_{up} = 15°$, $\sigma_{down} = 16°$ and $\rho_{up} = 0.55$, indicating that the data are again consistent with two populations of filament orientations. The classification in the subimage is shown in Fig. 9d.

Application of the methods described to a number of other micrographs of various qualities with a variety of noise levels and variable backgrounds produced good results in all but extremely noisy micrographs.

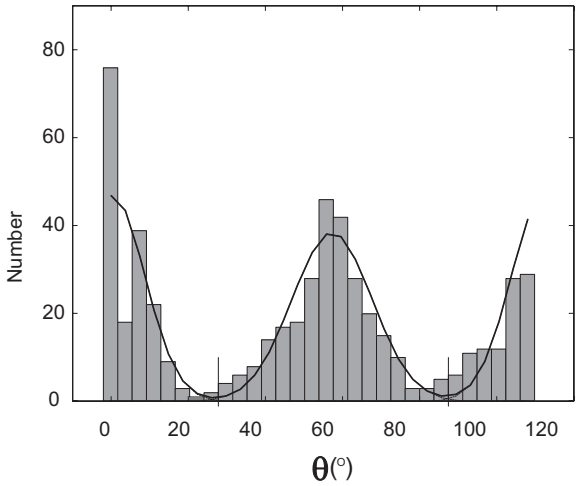

Figure 6: The histogram and mixture model for the frog sartorius muscle image.

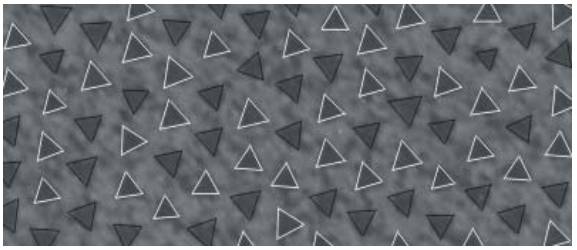

Figure 7: Outline of the triangular templates fitted to each filament, with white and black triangles denoting the classification into up and down orientations.

6. Conclusions

Electron micrographs of the A-band bare region of vertebrate muscle show cross-sections of the myosin filaments in a noisy and variable background. Automatic detection of the filaments and determination of their orientation is the first step in analysing the orientational disorder in the myosin lattice. Filament positions were determined by filtering with a psf that incorporates the lattice symmetry which is derived from a local region of the image. This is simpler than a previously implemented morphological algorithm and performs just as well. Filament orientations were determined by correlation with a suitable template and the orientations classified using a Gaussian mixture model. A comparison with manually classified orientations indicates

Table 1: Comparison of the automatic and manually determined orientations from the frog sartorius muscle micrograph.

Classification		Automatic orientations			
		up	down	bad	total
Manual orientations	up	283	1	11	295
	down	3	271	11	285
	bad	71	70	30	171
	total	357	342	52	751

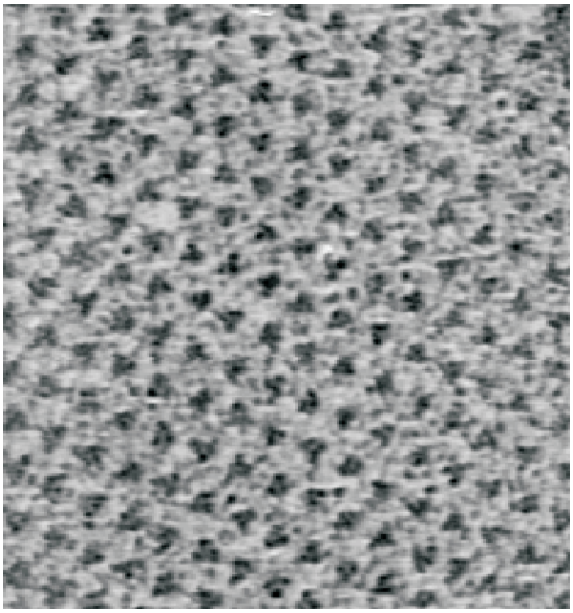

Figure 8: Electron micrograph of turtle muscle.

about 90% consistency, although this depends on the quality of the image. Application to a variety of micrographs indicates that the method is robust, even for quite noisy images that would be very difficult to analyse manually.

7. Acknowledgements

We are grateful to the N.Z. Marsden Fund for financial support and Pradeep Luther (Imperial College, London) for provision of the micrographs.

References

[1] J. M. Squire, "The structural basis of muscular contraction", *Plenum Press, London*, 1981.

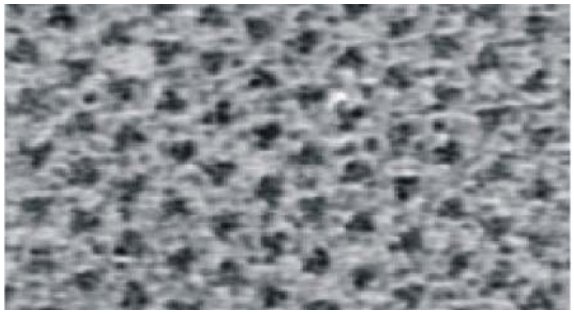

(a)

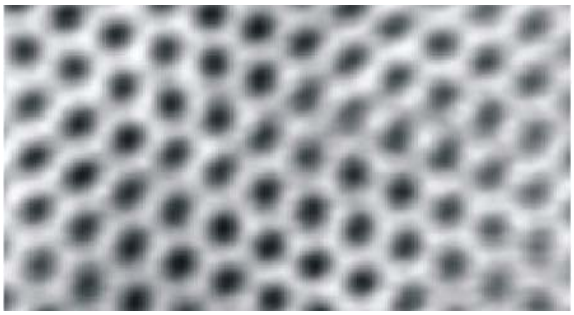

(b)

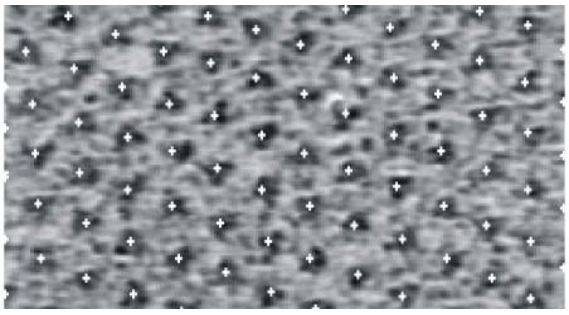

(c)

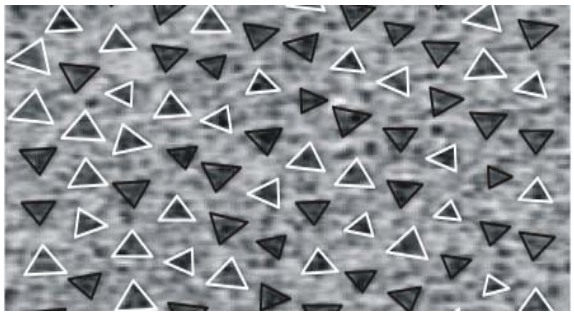

(d)

Figure 9: (a) A subimage of the turtle muscle micrograph, (b) the filtered subimage, (c) filament location and (d) the classification of filament orientations.

[2] P. K. Luther and J. M. Squire, "Three-dimensional structure of the vertebrate muscle A-band II. The myosin filament superlattice", *J. Mol. Biol*, **141**, pp. 409–439, 1980.

[3] R. P. Millane and A. Goyal, "Analysis of the disordered myosin lattice in muscle", *Fibre Diffraction Review*, **4**, pp. 6–11, 2000.

[4] B. Bödvarsson, S. Klim, S. Mortensen, M. Mørkebjerg, J. Chen, J.R. Maclaren, C.H. Yoon, P.K. Luther, J.M. Squire, A. Bainbridge-Smith, P.J. Bones and R.P. Millane, "Determination of myosin filament positions and orientations in electron micrographs of muscle cross-sections", in "Image Reconstruction from Incomplete Data III," P.J. Bones, M.A. Fiddy and R.P. Millane (Eds.), *Proc. SPIE*, **5562**, pp. 97–108, 2004.

[5] C.H. Yoon, J. Chen, J.R. Maclaren, B. Bödvarsson, S. Klim, S. Mortensen, M. Mørkebjerg, P.K. Luther, J.M. Squire, A. Bainbridge-Smith, P.J. Bones and R.P. Millane, "Automated analysis of electron micrographs of muscle cross-sections", in *Proc. Image and Vision Computing New Zealand 2004, Landcare Research, N.Z.*, pp. 173–179, 2004.

[6] L. Vincent, "Morphological grayscale reconstruction in image analysis: Applications and efficient algorithms", *IEEE, Trans. on Image Process.*, **2**, pp. 176–201, 1993.

[7] D. Dunn and W.E. Higgins, "Optimal Gabor filters for texture segmentation", in *IEEE, Trans. Image Process*, pp. 947–964, 1995.

[8] Y. Lee, T. Hara, H. Fujita, S. Itoh and T. Ishigaki, "Automated detection of pulmonary nodules in helical CT images based on an improved template-matching technique", in *IEEE, Trans. Medical Imaging*, pp. 595–604, 2001.